

# Photometric Survey of the Irregular Satellites

**Tommy Grav**<sup>1,2,3</sup>

*Institute of Theoretical Astrophysics, University in Oslo,  
Postbox 1029 Blindern, 0359 Oslo, Norway (tommy.grav@astro.uio.no)*

*&*

*Harvard-Smithsonian Center for Astrophysics,  
MS51, 60 Garden Street, Cambridge MA 02138 (tgrav@cfa.harvard.edu)*

**Matthew J. Holman**<sup>2,3</sup>

*Harvard-Smithsonian Center for Astrophysics,  
MS51, 60 Garden Street, Cambridge, MA 02138 (mholman@cfa.harvard.edu)*

**Brett J. Gladman**

*Dept. of Physics and Astronomy, University of British Columbia  
6224 Agricultural Road, Vancouver, B.C., V6T 1Z1, Canada (gladman@astro.ubc.ca)*

**Kaare Aksnes**

*Institute of Theoretical Astrophysics, University in Oslo,  
Postbox 1029 Blindern, 0359 Oslo, Norway (kaare.aksnes@astro.uio.no)*

Received \_\_\_\_\_; accepted \_\_\_\_\_

---

<sup>1</sup>Visiting Astronomer, Nordic Optical Telescope

<sup>2</sup>Visiting Astronomer, MMT Observatory

<sup>3</sup>Visiting Astronomer, Magellan Observatory

**Proposed Running Head:** Photometric Survey of Irregular Satellites

**Editorial Correspondence to:**

Tommy Grav

MS #51, 60 Garden Street

Cambridge, MA 02138

USA

Phone: 617-495-8752

Fax: 617-495-7093

email: [tgrav@cfa.harvard.edu](mailto:tgrav@cfa.harvard.edu)

## Abstract

We present BVRI colors of 13 Jovian and 8 Saturnian irregular satellites obtained with the 2.56m Nordic Optical Telescope on La Palma, the 6.5m Magellan Baade Telescope on La Campanas, and the 6m MMT on Mt. Hopkins. The observations were performed between December 2001 to March 2002. Nearly all of the known irregular satellites can be divided into two distinct classes based on their colors. One, the **grey** color class, has the similar colors to the C-type asteroid, and the other, the **light red** color class, has colors similar to P/D-type asteroids. We also find at least one object, the Jovian irregular J XXIII Kalyke, that has colors similar to the **red** colored Centaurs/TNOs, although its classification is unsecure.

We find that there is a correlation between the physical properties and dynamical properties of the irregular satellites. Most of the dynamical clusters have homogeneous colors, which points to single homogeneous progenitors being cratered or fragmented as the source of each individual cluster. The heterogeneous colored clusters are most easily explained by assuming that there are several dynamical clusters in the area, rather than just one.

By analyzing simple cratering/fragmentation scenarios, we show that the heterogenous colored S IX Phoebe cluster, is most likely two different clusters, a **neutrally** colored cluster centered on on S IX Phoebe and a **light red** colored cluster centered on S/2000 S 1. To which of these two clusters the remaining Saturnian irregulars with inclinations close to  $174^\circ$  belong is not clear from our analysis, but determination of their colors should help constrain this.

We also show through analysis of possible fragmentation and dispersion of the six known Uranian irregulars that they most likely make up two clusters, one centered on U XVI Caliban and another centered on U XVII Sycorax. We further show that, although

the two objects have similar colors, a catastrophic fragmentation event creating one cluster containing both U XVI Caliban and U XVII Sycorax would have involved a progenitor with a diameter of  $\sim 395$ km. While such an event is not impossible it seems rather improbable, and further we show that such an event would leave 5-6 fragments with sizes comparable or larger than U XVI Caliban. Given that the stable region around Uranus has been extensively searched to limiting magnitudes far beyond that of U XVI Caliban. The fact that only U XVI Caliban and the larger U XVII Sycorax have been found leaves us with a distribution not compatible with a catastrophic event with such a large progenitor. The most likely solution is therefore two separate events creating two Uranian dynamical clusters.

**Key Words:** Photometry; Satellite of Jupiter; Satellite of Saturn; Satellite of Uranus; Surfaces, Satellite

## 1. Introduction

The satellites of the giant planets in the outer system can be separated into two groups, the regular and irregular, based on their orbital characteristics. The orbits of the regular satellites are prograde, nearly circular, and very close to the equatorial plane of their host planet. It is commonly accepted that the regular satellites were created much like the solar system, forming from a circumplanetary disk of gas and dust. The irregular satellites, however, have highly inclined and eccentric orbits, with similar numbers of retrograde as prograde. They are typically small ( $\sim 10^2$ km) and have semimajor axes that are larger than the regular satellites. These orbital characteristics suggest that the irregular satellites formed outside of the circumplanetary disk and were subsequently captured.

The regular satellites have been studied extensively through both ground-based and space-based platforms. Aside from the scattered light from their host planets, the size and brightness of the regular satellites make them easy targets for even the smallest ground-based telescopes. The irregulars, however, are sufficiently fainter that, until recently, the sample of known objects has been severely limited. N I Triton, with its small, circular but retrograde orbit, was discovered in 1846 by W. Lassell (Lassell 1846). The first distant irregular satellite, S IX Phoebe, orbiting around Saturn, was discovered by W. Pickering in 1889. These, along with eight Jovian (J VI Himalia, J VII Elara, J VIII Pasiphae, J IX Sinope, J X Lysithea, J XI Carme, J XII Ananke and J XIII Leda) and one other Neptunian (N II Nereid) irregular satellites were the only ones known.

Recent discoveries have dramatically increased the census of irregular satellites. In 1997-1999, (Gladman *et al.* 1998, 2000) reported the discovery of five Uranian irregulars. In 1999-2000 a dozen new irregular satellites were discovered around both Jupiter (J XVII Callirrhoe to J XXVII Praxidike and S/2000 J11) (Scotti *et al.* 2000; Sheppard *et al.* 2000, 2001; Green 2002) and Saturn (S/2000 S 1-12) (Gladman *et al.* 2001), more than

tripling the number of known irregulars in the Solar System. Most recently, the discoveries of another 11 Jovian irregular satellites (S/2001 J 1-11) (Sheppard *et al.* 2002) and another Uranian (S/2001 U 1) (Holman *et al.* 2002) were reported.

Several scenarios have been proposed for the origin of the irregular satellites, most concentrating on some type of capture of objects from heliocentric orbit. These objects may be temporarily captured in orbits around the giant planets, by passing through the interior Lagrange point,  $L_2$ , with a low velocity (Heppenheimer 1975). The capture is only temporary, since no energy is lost in the transfer from heliocentric to planetcentric orbit. Temporary capture typically lasts only 10 – 100 orbits (Byl and Ovenden 1975; Heppenheimer and Porco 1977). An energy dissipation mechanism is therefore needed to make the capture permanent. The fact that the first seven Jovian irregular satellites form two dynamical groups, the progrades and the retrogrades, was recognized early. Kuiper (1956) first suggested that these two known classes of Jovian satellites were most likely the result of two separate events rather than seven (J XIII Leda was not yet discovered). Colombo and Franklin (1971) proposed that the capture was due to fragmentation during a single collision between an outer Jovian satellite and an asteroid. The fragments of the larger satellite would comprise the prograde Jovian group, while the fragments of the asteroid would make up the retrograde group. Heppenheimer and Porco (1977) studied how a rapid increase of a planet’s mass during formation could temporarily captured objects into bound irregular satellites. Pollack *et al.* (1979) proposed yet another capture mechanism. They envisioned that the two clusters were indeed fragments of separate parent bodies, but that the parent bodies were captured by gas drag from an extended gas envelope around the giant planet. They assumed that one pass through the gas envelope was sufficient to lower the progenitors velocities enough for them to be permanently captured. The gas envelope collapsed, at least locally, shortly after the capture of the two progenitors ( $\leq 10$  years) ensuring that the gas drag did not cause their orbits to spiral into the planet. Pollack

*et al.* also raised the point that the two progenitors may have been fragmented after being captured due to the dynamic pressure of the gas exceeding the progenitor's strength. They demonstrated that these fragments would stay gravitationally bound to each other and that a close encounter or collision was needed to disperse them. Recently Cúk and Burns (2001) have taken the gas drag model one step further by assuming a flattened disk around a proto-Jupiter instead of the extended gas envelop used by Pollack *et al.* (1979). These theories all imply different time scales and satellite ages.

Gladman *et al.* (2001) found that almost all of the newly discovered irregulars also cluster in easily discernible groups. They also found more clusters than the two (pro- and retrograde) initially envisioned. The new Jovian satellites seem to divide the formerly dispersed retrograde group into at least two subclusters based on their mean orbital elements. In addition J XVIII Themisto and J IX Sinope (the former prograde, the later retrograde) now appear as single objects that indicate other yet undiscovered clusters. The Saturnian irregulars can be divided into three clusters (two prograde and one retrograde) again based on their mean orbital elements. It is unclear if S/2000 S 8 falls into the retrograde S IX Phoebe cluster. The five known Uranian irregular satellites have been established to inhabit one or two retrograde clusters. Gladman *et al.* (2001) argue that this orbital clustering suggests that most of the current irregulars are fragments from the collisional disruption of earlier captured progenitor satellites rather than individual satellite captures. A test of this break-up model was proposed. If the irregulars are collisional fragments the broad-band colors within a cluster should be homogeneous.

There exists color photometry, lightcurve, and reflectance spectra for most of the large irregular satellites of Jupiter and Saturn, but little photometry has been reported on the recent discoveries. Gladman and Boehnhardt (2000) reported BVRI magnitudes of J XVII Callirrhoe (formerly designated S/1999 J 1). BVR colors of the Uranian irregular

satellites U XVI Caliban and U XVII Sycorax have been measured by Maris *et al.* (2001) and Romon *et al.* (2001). Schaefer and Schaefer (2000) observed N II Nereid and determined its UBVRI colors.

Although the physical properties of the larger, previously known Jovian irregular satellites have been studied in more extensively, the reported measurements are sometimes contradictory. Degewij *et al.* (1980) looked at the photometric properties of the outer planetary satellites and found that the outer Jovian satellites resemble C-type asteroids. Degewij (1980) also measured the near-infrared reflectance of J VI Himalia and S IX Phoebe in the 0.3 to 2.2  $\mu\text{m}$  and confirmed that they too resemble C-type asteroids. Tholen and Zellner (1983, 1984) reported multicolor observations of six Jovian irregular satellites, as well as S IX Phoebe, and found that all the progrades resemble C-type asteroids. The retrogrades were found to be more diverse in color, with J VIII Pasiphae and S IX Phoebe looking like C-type asteroids. J IX Sinope was found to be very red, while J XI Carme showed a reflectance spectrum that was flat, but with a strong upturn in the ultraviolet. Tholen and Zellner (1983, 1984) speculated that J XI Carme might be showing low-level cometary activity with CN emission at 0.388  $\mu\text{m}$ .

Luu (1991) reported VRI colors, light curves, and reflectance spectra for J VI-XIII. She concluded that the satellites resemble a mixture of C- and D-type asteroids. Similarities between the satellites and the Trojan asteroids were investigated and found to be consistent with the hypothesis put forth by Kuiper (1956) that the two groups of objects (pro- and retrograde) share a common origin. However, by comparing the lightcurves of 6 Jovian irregular satellites and 14 Trojan asteroids Luu (1991) found that the satellites lack the extreme shapes of the Trojans. The physical properties of the large Jovian irregular satellites are generally consistent with, but do not prove, the capture origin theory proposed by Pollack *et al.* (1979).



In September 1998, six of the then known eight Jovian irregular satellites were detected in the Two-Micron All Sky Survey (Sykes *et al.* 2000). The near-infrared colors ( $J$ ,  $H$  and  $K$ ) of the prograde satellites were found to be consistent with the hypothesis that these objects are fragments of a captured C-type asteroid. The retrograde satellites in general showed considerable diversity. The failure to detect J XII Ananke is significant, since it implies a visible to near-infrared reddening close to that of prograde J VI Himalia and very different from the other retrograde satellites. This suggests that the retrograde Jovian satellites are fragments of a more heterogeneous parent body than the prograde satellites. This result was confirmed by Rettig *et al.* (2001) who performed a BVR color survey of the eight large Jovian irregular satellites. They noted that the retrograde group appeared redder and more diverse in both the  $B - V$  and  $V - R$  colors than the prograde group.

Gladman *et al.* (2001) showed that the fragmentation idea proposed by Pollack *et al.* (1979) was likely incomplete. Capture and subsequent break-up by gas drag would mean that smaller fragments, which are more coupled to the gas, should experience faster orbital evolution spiraling in towards the planet and circularizing their orbits. This is contradicted by S IX Phoebe which is the largest and the inner-most of its cluster. Also the Uranian U XVI Caliban and U XVII Sycorax (the largest irregular satellite) are two of the three closest of their cluster. Gladman *et al.* (2001) favored the idea that each cluster is produced by disruption of the parent body due to collisional events well after the capture.

In this paper we present BVRI photometry of a number of the irregular satellites of Jupiter and Saturn from observations performed at the Nordic Optical Telescope, MMT Observatory and Magellan Observatory. We further examine the dispersion of colors and investigate the correlation between color and dynamical class in order to better understand the physical and dynamical structure of the irregular satellites. By comparing the physical and dynamical properties we can determine whether a dynamical cluster has similar physical

properties. A homogeneous cluster will point to a common progenitor for its members (the capture of several bodies with similar surface composition is also a possibility, but this indicate that there are inclinations for which capture is preferred, which seems unlikely), while a heterogeneous cluster makes additional or other explanations necessary.

By determining the orbital and physical properties of the irregular satellites it is possible to better establish the number of dynamical clusters around each planet. Gaining such a census of the number of clusters, and thus the number of possible progenitors, is necessary to determine the time scale over which capture of the irregular satellites happen. This will help distinguish between the different types of capturing theories.

## 2. Observations

The known irregular satellites have red magnitudes in the range  $R \sim 16 - 24$ , with all the newly discovered objects fainter than  $R \sim 20$ . For the fainter objects medium to large-sized telescopes are needed to acquire sufficient signal-to-noise ratio to accurately determine their colors. We acquired time on three different telescopes: the 2.51m Nordic Optical Telescope (NOT) on La Palma, the 6.5m MMT on Mt. Hopkins, Arizona and the 6.5m Magellan Observatory at Las Campanas, Chile. The circumstances of the observations are given in Table 1.

Most of the observations were performed under photometric conditions at the NOT using the ALFOSC camera (Sørensen and Nørregaard 1996). The image scale of this instrument with its Tektronix 2048x2048 pixel charge-coupled device (CCD) is 0.189 arcsec per  $15\mu\text{m}$  pixel. A set of broad-band Bessel BVRI filters were used for all the NOT observations.

A number of observations were also performed under photometric conditions at the

Magellan Baade 6.5m telescope in Chile using MagIC. The image scale of this instrument with its SITe 2048x2048 pixel, 4 amplifier CCD is 0.069 arcsec per  $24\mu\text{m}$  pixel. The MagIC has a set of Harris BVRI filters that were used for the observations.

Additional observations were performed under photometric conditions at the MMT 6.5m telescope on Mt. Hopkins, Arizona, using the MiniCam (a prototype of Megacam; McLeod *et al.* 2000). The Minicam has two 2048x4608 pixel CCDs, which in 2x2 binned mode, gives 0.091 arcsec per  $27\mu\text{m}$  pixel. The two chips are mounted side by side with a 1mm (3.5 arcsec) gap. The MMT has a set of Harris BVRI filters that were used for the observations.

The irregular satellites move across the sky at rates of 5 – 12 arcsec per hour. Thus, the exposure time were limited to avoid trailing loss. Since photometry of field stars is needed to do aperture photometry (see next section), we need to track at sidereal rates, rather than tracking at the satellites' rates. With seeing of 1.0 – 1.5 arcseconds, the maximum exposure time is limited to 240s for a Jovian irregular satellite and to about 300s for a Saturnian. Several images were therefore taken in each filter. The images were then shifted and co-added to increase the signal-to-noise ratio and to avoid trailing losses.

### 3. Data Reduction

All the images were overscan corrected, bias subtracted, and flat field corrected to remove differences in the sensitivity over the CCD. The bias was created by averaging 10-15 zero-time exposure. The flatfield frames were created by taking the median of a series of short exposures of the evening/morning twilight or of an illuminated white screen inside the telescope dome. This removed most of the irregularities found on the CCD, producing very uniform images with less than 1% variability across the CCD.

The photometry was flux calibrated using numerous standard stars (Landolt 1992). Extinction coefficients and transformation equations were determined for each night. The DAOPHOT package (Stetson *et al.* 1990) in IRAF (Tody 1986, 1993) was used to determine the instrumental magnitudes, transformation equations, photometry, and colors of the objects.

Since many of the satellites are very faint and have errors dominated by sky noise, the technique of aperture correction was used (Howell 1989). The aperture sizes were picked to ensure that the inner aperture covered about one and a half times the full-width at half maximum (FWHM) of the psf of the object. This aperture size insure that a maximum signal-to-noise ratio is achieved for the objects (Dacosta 1992). Thus, a aperture radius of 9 pixels was used for the data taken at NOT and MMT ( $\sim 1.7$  and  $\sim 0.9$  arcseconds respectively), while 12 pixels ( $\sim 0.9$  arcseconds) was used for the Magellan observations. For the outer aperture 2-3 times the FWHM of the psf was used and experimentation showed that 25 pixels worked well for all the data. For the determination of the sky background an annulus 10 pixels wide with an inner diameter of 30 pixels was used. The aperture correction magnitude varies with seeing, but is generally in the range  $\Delta m \sim 0.1 - 0.3$  with errors of  $\pm 0.01 - 0.03$ .

In some of the images taken using the I-band filter, severe fringing effects made reduction of the images difficult. Since the fringing effects were confined to the outer parts of the CCD, only the images where the positional uncertainties of the target were great did it effect the data reduction. By summing the available images taken using the I-band filter it was possible to create a fringing flat that removed most of the fringing, resulting in images with less than 3% variability across the CCD.

#### 4. Photometric Results

In this survey BVRI photometry and the associated colors were determined for 13 Jovian and 8 Saturnian irregular satellites, out of the 20 Jovian and 13 Saturnian irregular satellites known at the time of observation. Since most of the observations were performed at the 2.51m Nordic Optic Telescope at La Palma, the survey is mostly limited to the objects brighter than  $m_V = 23.0$ .

Table 2 gives the absolute magnitude, normalized to unit heliocentric and geocentric distance and zero degree phase angle (Bowell *et al.* 1989), the observed  $V$ -magnitude, and the  $B - V$ ,  $V - R$ , and  $V - I$  colors with their associated errors. The corresponding solar colors are approximately  $B - V = 0.67$ ,  $V - R = 0.37$  and  $V - I = 0.71$  (Hartmann *et al.* 1982).

The  $B - V$  vs  $V - R$  colors are shown in Fig. 1 similar to the plots that have become the norm for identifying structures in the color distribution. Rettig *et al.* (2001) used a similar plot to show the difference in colors between the prograde and retrograde populations of the Jovian irregular satellites. Figures 1-3 includes all the objects observed in this survey, as well as colors reported by for J VI Himalia, J VII Elara, J XIII Leda (Rettig *et al.* 2001) and the two Uranian U XVI Caliban and U XVII Sycorax (Maris *et al.* 2001; Romon *et al.* 2001). Figure 4 also includes the Centaurs and TNOs for which  $B - V$  and  $V - R$  colors with uncertainties below 0.05 magnitudes are available.

Figure 1 confirms the distribution of colors found by Rettig *et al.* (2001). The objects can be roughly separated into two distinct classes based on their colors. One which is essentially **grey** in color (the objects have sun-like colors) and one which will be hereafter called **light red**. The  $B - V$  vs.  $V - I$  plot in Fig. 2 and  $V - R$  vs.  $V - I$  plot in Fig. 3 confirm this distribution. Note that one object changes classification between the plots. We attribute this to an underestimation of the error of the I-band photometry due to fringing

effects. It should also be noted that there exists few estimates of variation in the colors due to variation in surface properties. S IX Phoebe is a good example of an irregular satellite that has a large bright spot on one side of it’s surface (Simonelli *et al.* 1999). How this bright spot affects the color as S IX Phoebe rotates has not yet been investigated.

These two classes should not be confused with the two different classes named **grey** and **red**, found in the Centaur/TNO population by Tegler and Romanishin (1998, 2000). Figure 4 shows that both the **grey** and **light red** classes as defined in this paper coincide with what Tegler and Romanishin (1998, 2000) call the **grey** class.

## 5. Dynamical Class and Colors

When comparing colors of objects within a dynamical cluster it becomes evident that for most clusters the individuals members have similar colors, suggesting a common progenitor. Figure 5 shows a polar plot of the mean semimajor axis  $a$ , normalized to the Hill sphere,  $R_H$ , for each parent planet, and mean inclination  $i$  (Pollack *et al.* 1979; Gladman *et al.* 2001, ;JPL Solar System Dynamics website ([ssd.jpl.nasa.gov](http://ssd.jpl.nasa.gov))). The different Jovian dynamical clusters are immediately apparent, while the more disperse Saturnian and Uranian clusters are harder to spot. Objects for which photometry has been performed have been colored according to their apparent color class, *blue* for **grey** (C-type) colored objects and *red* for **light red** (P- or D-type) colored objects. The unobserved objects have black symbols.

Assuming that the most massive body in each cluster is close to the original orbit before a catastrophic collision, the colored areas in Fig. 5 show the possible dispersion of fragments in semimajor axis and inclination. We generated these dispersion areas by adding fixed length velocity vectors with random directions to the velocity vector of the

largest member of each cluster, using that objects mean orbital elements and assuming that the collision occurs at a given orbital phase and is an relative small impulse. Given for each resulting velocity vector, new orbital elements are calculated. The cluster of points can be understood in the limit of small velocity changes. We assume typical dispersion velocity  $\Delta \mathbf{v} = \Delta \mathbf{v}_S + \Delta \mathbf{v}_T + \Delta \mathbf{v}_W$ , where the velocity vector has been split into three components.  $\Delta \mathbf{v}_W$  gives the component perpendicular to the orbital plane of the satellite, while  $\Delta \mathbf{v}_S$  and  $\Delta \mathbf{v}_T$  are the components along and at right angles to the radius vector,  $\mathbf{r}$  of the satellite from the planet. The dispersion in  $a$ - $i$  phase space is then given by (Roy 1988)

$$\Delta a = \frac{2}{n\sqrt{1-e^2}} \left( e \sin f \Delta v_s + \frac{p}{r} \Delta v_T \right) \quad (1)$$

and

$$\Delta i = \frac{r \cos u}{na^2 \sqrt{1-e^2}} \Delta v_W \quad (2)$$

where  $f$  is the true anomaly,  $p = a(1 - e^2)$  and  $u = f + \bar{\omega} - \Omega = f - \omega$ .

All of the known clusters are made up of one large and several smaller bodies. The smallest mass difference between the largest and next largest bodies can be found in the Saturnian 45°-inclination cluster (mass-ratio  $\sim 5$ ) and the potential Uranian cluster containing both U XVII Sycorax and U XVI Caliban (mass-ratio  $\sim 7$ ). Evaluating the center of mass for these two show that dispersion areas centered on the “*center of mass*” are near identical to the dispersion areas centered on the largest body of the cluster.

The speed of the fragments and the true/mean anomaly of the progenitor at impact have been adjusted to show plausible divisions of the objects into clusters. While a more careful analysis that accounts for post-collisional orbital evolution and the probability of impact at different orbital phase is beyond the scope of this paper, the scatter plots provide an zeroth-order approximation of the dispersion velocities needed to create the clustering structure seen in the irregular satellites around all the giant planets.

Rettig *et al.* (2001) determined colors for the 8 brightest Jovian irregular satellites and noted that the colors for the retrograde were less homogeneous and generally redder than those of the four prograde irregular satellites. In this survey we have observed 7 more retrograde and one prograde, as well as J VIII Pasiphae, J IX Sinope, J XI Carme and J XII Ananke. We find that the retrograde dynamical cluster centered on  $149^\circ$  inclination is indeed severely heterogeneous, while the cluster around J XI Carme is homogeneous with objects in the **light red** color class.

We also observed eight Saturnian irregular satellites and found that the two prograde clusters centered on  $34^\circ$  and  $46^\circ$  were found to be homogeneous with **light red** colors like the D-type asteroids. The retrograde cluster containing S IX Phoebe was however heterogeneous, with one **grey** colored object (S IX Phoebe) and one with **light red** color (S/2000 S 1).

In the following sections we examine in more detail the different clusters and propose some possible theories for the origin of each dynamical cluster.

### 5.1. The Jovian Prograde ( $28^\circ$ inclination) cluster

The Jovian prograde  $28^\circ$  inclination-cluster are all clustered in the **grey** color class with weighted mean colors  $B - V = 0.66 \pm 0.02$  and  $V - R = 0.36 \pm 0.01$ . Of the five known members of this cluster only J X Lysithea was observed during this survey, while the colors of J VI Himalia, J VII Elara and J XIII Leda were taken from Rettig *et al.* (2001). We did not observe S/2000 J 11, which remains the only Jovian irregular satellite discovered in 2000 that has not been recovered. The colors of J X Lysithea reported in this paper are consistent with colors reported by Luu (1991) and Rettig *et al.* (2001). The **grey** colors of the prograde cluster imply that they have surfaces similar to that of C-type asteroids.



Cúk and Burns (2001), studying the gas-assisted capture of irregular satellites, have found that the progenitor of the prograde cluster may have originated from the Hilda region, about 4AU from the Sun. The Hilda family is dominated by P- and D-type asteroids, but due to a spectral slope - asteroid size correlation, the largest members of the family 153 Hilda (with a diameter of 170km) and 334 Chicago (with a diameter of 156km) are possibly C-type asteroids (Dahlgren *et al.* 1997). It is usually assumed that the progenitor of a fragmented dynamical cluster had roughly twice the size of the clusters largest member today. J VI Himalia with its diameter of  $\sim 85$ km implies a progenitor body of similar size as 153 Hilda and 334 Chicago. Jarvis *et al.* (2000) however classify J IV Himalia as an F-class asteroid, a subclass of C, and propose that it originated as part of the Nysa asteroid family. The spectroscopic data collected by Jarvis *et al.* (2000) however show evidence of absorption features at  $0.7 \mu\text{m}$ , which is only weakly or non-evident in other F-class asteroids (Sawyer 1991).

Figure 5 shows the a-i phase space dispersion with a fragmentation speed of 150 m/s centered on J VI Himalia, assuming that the collisional event happened at pericenter. This dispersion speed is approximately twice the escape velocity, at  $v_e \sim 102$ m/s, and clearly indicates that the five objects in the vicinity are fragments of a common progenitor, that most likely originated in the outer part of the Main Asteroid Belt.

## 5.2. The Jovian IX Pasiphae and XII Ananke ( $149^\circ$ inclination) cluster(s)

The  $149^\circ$  cluster is currently the group with the greatest number of members. This cluster is dynamically the most diverse of the known Jovian clusters with inclinations ranging from  $147.1^\circ$  to  $152.7^\circ$ . This is a factor of 3 larger than the dispersion of the prograde  $28^\circ$  cluster and a factor of ten larger than the dispersion of the  $165^\circ$  cluster. The

149° cluster also has the largest range of semimajor axis, about 3 times more dispersed than the 28° cluster and 6 times more than the 165° cluster. The orbital mean elements suggest two distinct dynamical clusters instead of one, one centered on J IX Pasiphae and one centered on J XII Ananke. As can be seen in Fig. 5 there appears to be a gap in the semimajor axis between the two clusters. J VIII Sinope, with its mean orbital inclination of 158.1°, seems to be an independent capture of an object that has not been fragmented.

This paper presents colors for all seven members of this cluster that were known at the time of observation, but for J XXII Harpalyke the  $B - V$  color could not be determined, due to its faintness. The results of the observations can be seen in Table 2 and Fig. 1-3. The cluster has a very disperse set of colors with weighted mean  $B - V = 0.75 \pm 0.04$  and  $V - R = 0.41 \pm 0.08$ . Both J IX Pasiphae and J XII Ananke have been observed earlier (Degewij *et al.* 1980; Tholen and Zellner 1984; Luu 1991; Rettig *et al.* 2001). The observations of J IX Pasiphae given in this paper are in good agreement with these previous observations and the weighted mean colors of all available observations give the colors  $B - V = 0.71 \pm 0.05$ ,  $V - R = 0.39 \pm 0.02$  and  $R - I = 0.75 \pm 0.03$ . This places it in the **grey** color class.

Our observations of J XII Ananke are consistent with other observations in the  $V - R$  color, but our  $B - V$  color is slightly high at  $B - V = 0.90 \pm 0.06$  compared to  $0.76 \pm 0.03$  (Rettig *et al.* 2001). Our results differ from those of Rettig *et al.* only at the  $2\sigma$  level and could be the result of slight contamination by background source or statistical fluctuations. The weighted mean colors of all the observations give  $B - V = 0.77 \pm 0.03$ ,  $V - R = 0.42 \pm 0.02$  and  $V - I = 0.83 \pm 0.04$ , and places J XII Ananke right on the border between the **grey** and **light red** color classes. Further observations with higher accuracy are needed to determine the color of this object, but currently the observations seems to favor it as a **light red** object, rather than **grey**.

We are thus left with a rather confusing collection of orbits and colors. J IX Pasiphae has a **grey** color, while the irregular satellites with similar orbits (J XVII Callirrhoe and J XIX Magaelite) have **light red** colors. For the objects clustered around J XII Ananke the problem is the same, but reversed, with J XII Ananke exhibiting a **light red** color and J XXII Harpalyke, J XXVII Praxidike and J XXIV Iocaste having **grey** colors. It should again be stressed that the color of J XII Ananke is right on the border between the two classes of colors. Further and more accurate observation is necessary to determine its color beyond doubt. Saha and Tremaine (1993) demonstrated that both J VIII Sinope and J IX Pasiphae are trapped in secular resonances. It is reasonable to assume that significant orbital evolution has moved the object in this area of phase space away from their immediate post-fracture orbits, trapping some in the secular resonances. A more detailed study of both the physical and dynamical properties of these bodies are needed to better understand the mechanism that govern the evolution of these bodies.

It should be noted that it is possible to find dispersion ellipses, using dispersion velocities of 200m/s, that create homogeneous clusters. This however create rather arbitrary combination of objects that does not seem to have anything but colors in common.

### 5.3. The Jovian XI Carme (165° inclination) cluster

The objects of the Jovian XI Carme cluster has very little dispersion in their mean orbital elements of semimajor axis and inclination. Three of the six known objects from this cluster were observed during this survey. Two, J XI Carme and J XX Taygete, lay in the **light red** color class, while J XXIII Kalyke has colors more consistent with the **red** class defined by Tegler and Romanishin (1998, 2000). J XXIII Kalyke is the only object in the sample to exhibit this redness. But looking at the  $V - I$  color of J XXIII Kalyke it is seem to be part of the **light red** class. Why J XXIII Kalyke has such a red  $V - R$  color, while

it's  $V - I$  color is moderate is uncertain, but it is possible that the moderate  $V - I$  color is due to underestimated fringing effects. The observation of J XXIII Kalyke at the NOT on Jan 24. 2002, indicate that the  $V - I$  color could be high ( $0.96 \pm 0.16$ ). Two separate observation was taken of J XXIII Kalyke to confirm the high  $V - R$  color and both are consistent within the estimated errors, but further observations are needed to confirm the **red** color.

The J XI Carme cluster is consistent with a collisional event giving the fragments speeds at  $\sim 30\text{m/s}$ , which is just beyond the escape velocity of J XI Carme ( $v_e \sim 28\text{m/s}$ ). It is by far the thightest of the dynamical clusters and seems to have been very little post-fracture orbital evolution. We propose that the J XI Carme cluster has a D-type progenitor, most likely from the Hilda or Trojan families. How J XXIII Kalyke fit's into the cluster is still very much an open question. The **red** color points to an origin in the Centaur/TNO population and it is possible that J XXIII Kalyke is a surviving fragment of the impactor that caused the fragmentation of the J XI Carme progenitor, although it seems very unlikely that such a fragment would have a post-collisional orbit exactly that of the progenitor it impacted.

#### 5.4. The Saturnian $34^\circ$ and $46^\circ$ inclination clusters

The two prograde Saturnian clusters, with mean orbital inclinations around  $34^\circ$  and  $46^\circ$  also have fairly tightly clustered colors. They both lay in the **light red** class. The  $34^\circ$ -cluster has weighted mean colors of  $B - V = 0.91 \pm 0.05$  and  $V - R = 0.48 \pm 0.01$ . The moderate dispersion in the  $B - V$  color is due to the high uncertainty in the measurements of this color in all the three objects in this cluster that was measured. The  $46^\circ$ -cluster has weighted mean colors of  $B - V = 0.79 \pm 0.01$  and  $V - R = 0.51 \pm 0.02$ .

It is important to mention that although the two clusters seem to be homogeneous, there are significant uncertainties. S/2000 S 10, belonging to the  $34^\circ$  inclination cluster, is clearly in the **light red** color class when looking at the  $B - V$  vs.  $V - R$  plot in figure 1. It has however a very low  $V - I$  color at  $0.61 \pm 0.12$ , which puts it in the **grey** color class in the  $B - V$  vs.  $V - I$  (figure 2) and  $V - R$  vs.  $V - I$  (figure 3) plots. This is most likely due to the combination of the faintness of S/2000 S 10, with a  $V$  magnitude at  $23.90 \pm 0.05$ , and the fringing effects that show up in the  $I$  filtered images when doing long exposures. It is likely that the formal errors for the  $V - I$  color of S/2000 S 10, as given in table 2, is underestimated. We have therefore decided to disregard the  $V - I$  color of this object and classify it as a **light red** colored object. More observations are necessary to confirm this classification.

Both these dynamical clusters are neatly confined. All the objects in the  $34^\circ$  inclination cluster easily fit inside the dispersion ellipse given fragment speeds of 50m/s centered on S/2000 S 11, which is the biggest member of the cluster with a diameter of 13 km. Using this diameter, S/2000 S 11 has an escape velocity of only  $\sim 5$ m/s.

While the  $46^\circ$  inclination cluster is physically homogeneous, a large dispersion velocity is needed, at 350m/s centered on its largest member, S/2000 S 3, to be able to fit a dispersion area that contains them all. S/2000 S 3, with a diameter of 16 km, has an escape velocity of  $v_e \sim 18$ m/s. The large dispersion velocity could be due to a close encounter with a large object that was subsequently cleared away. It was recently reported that there has been discovered possible secular resonant motion in three of the four known members of this dynamical cluster (Carruba *et al.* 2002; Cúk *et al.* 2002). These secular resonances may have caused significant post-fragmentation orbital evolution that could be behind the large dispersion of orbital elements in this cluster.

### 5.5. The Saturnian IX Phoebe (174° inclination) cluster

Only two of the four known members of the 174° inclination cluster were observed. S IX Phoebe was found to lay in the **grey** class, while S/2000 S 1 is part of the **light red** color class.

The color of S IX Phoebe found here is consistent with  $B - V$  observations from Degewij *et al.* (1980) and Tholen and Zellner (1983). Degewij *et al.* (1980) also reported a single  $V - R$  observation of  $0.66 \pm 0.02$ , which differs significantly from the color found in this survey. Spectral observations of S IX Phoebe in the  $0.33 - 0.92 \mu\text{m}$  region at two subsequent nights by Buratti *et al.* (2002) both show essentially flat and grey spectra, which is consistent with the color observations in this paper.

The size distribution of the S XI Phoebe cluster, with one large and several small bodies, points to one or more cratering events. There is an upper limit on the energy density of a collision for a cratering event, given by  $E/M_T \sim 10^2 \text{J/kg}$ , where  $E$  is the kinetic energy of the impactor and  $M_T$  is the mass of the target (Fujiwara *et al.* 1989). Energies larger than this will lead to fragmentation of the target, leaving a different mass distribution than found in the S IX Phoebe cluster. Assuming that such event only knocked loose a piece of similar size of S/2000 S 1 ( $\sim 7 \cdot 10^{-4} M_T$ ) and that 10% of the energy is converted into kinetic energy for the piece (Fujiwara *et al.* 1989), a maximum speed of  $\sim 170 \text{m/s}$  is achieved. For objects with similar sizes as S/2000 S 12 ( $\sim 3 \cdot 10^{-6} M_T$ ), using the same arguments, yield a maximum dispersion speed of  $\sim 2.6 \text{km/s}$ . It is important to remember that these are generous upper limits, assuming that the maximum energy possible for a cratering event and also assuming that only one piece is knocked out, with all the kinetic available being used in accelerating it. If we assume that both S/2000 S 7 and S/2000 S/12 (for a total mass of  $\sim 6 \cdot 10^{-6} M_T$ ) were part of the same event, we get upper dispersion

velocities of  $\sim 1.8\text{km/s}$ .

Maximum dispersion in semimajor axis is achieved when the fragmentation/cratering happens at or close to the orbits pericenter. Dispersion speeds of over  $300\text{m/s}$  is needed to include S/2000 S 1 in a dispersion area centered on S IX Phoebe. It is very unlikely that it is a piece that has been carved of S IX Phoebe due to cratering. The **light red** surface color of S/2000 S 1 further supports this, meaning that S/2000 S 1 probably is the largest remaining piece of a catastrophic fragmentation of another progenitor. On the other hand, it is possible to create a dispersion ellipse using a dispersion velocity of  $\sim 250\text{m/s}$ , that includes both S/2000 S 7 and S/2000 S 12. By increasing this to dispersion velocity to  $\sim 350\text{m/s}$  and assuming that the cratering happened at apocenter rather than pericenter S/2000 S 9 can be included as well. It is therefore possible that these three irregular satellites are pieces from a cratering event on S IX Phoebe. While this dispersion velocity is high enough to create dispersion areas that include S/2000 S 1, it is not included in this case as the cratering happens at apocenter it results in a larger dispersion in inclination and thus reducing the dispersion in semimajor axis. It is also possible, using dispersions velocities of  $\sim 250\text{m/s}$  and an event close to  $M = 220^\circ$ , to create a dispersion area centered on S/2000 S 1 that includes all three of the irregular satellites, S/2000 S 7, S/2000 S 8 and S/2000 S 12.

We are therefore left with the conclusion that there is are two rather than one dynamical cluster, both with inclinations  $\sim 174^\circ$ . It is however not clear to which of these two clusters the three small irregular satellites, with diameters of  $\sim 2 - 4\text{km}$ , that reside in orbits between S IX Phoebe and S/2000 S 1 belong to. Determining their colors would help determine which of the two progenitors they most likely are the result of.

It should also be noted that it is possible that orbital evolution after fragmentation of **one single** progenitor is behind the current orbital distribution. This suggest that

S IX Phoebe either moved inwards or S/2000 S 1 diffused outwards. Both these scenarios seems unlikely as no secular resonances have been reported to be present in this region around Saturn. The fact that the two objects observed in this survey have such different colors, also support the idea of two rather than one dynamical cluster in the vicinity.

### 5.6. The Uranian Irregular Satellites

The six known Uranian irregular satellite all have similar orbital elements, but with a rather large dispersion. It has been speculated that these irregulars make up several dynamical clusters, but no clear evidence of this has been found. Only U XI Caliban and U XII Sycorax have had their  $B - V$  and  $V - R$  colors determined (Maris *et al.* 2001; Romon *et al.* 2001), and both have **light red** colors.

Looking at the possible dispersion caused by fragmentation makes it clear that there is likely more than one dynamical cluster, unless the irregulars have had significant orbital evolution after fragmentation. Using dispersion velocities of 75 and 115m/s centered on U XVI Caliban ( $v_e \sim 45\text{m/s}$ ) and U XVII Sycorax ( $v_e \sim 87\text{m/s}$ ), respectively, the six Uranian are divided into two clusters (see Fig. 5). U XVIII Prospero and U XIX Setebos are then part of the U XVII Sycorax cluster, while U XX Stephano falls in the U XVI Caliban cluster. The new S/2001 U 1 does not fit into either cluster, but it's current mean orbital elements (which are still rather uncertain) suggest that it is part of the U XVII Sycorax cluster. It is possible to fit all the Uranian irregulars inside a dispersion area centered on U XVII Sycorax (the biggest of the Uranian irregulars with a diameter of  $\sim 95\text{km}$ ), using a dispersion velocity of  $\sim 250 - 300\text{m/s}$  and a collisional event close to apocenter. To create such a dispersion velocity for U XVI Caliban alone, a fragmentation caused by a event with energy density  $E/M_T \sim 5 \cdot 10^4\text{J/kg}$  is needed (again assuming that 10% of the energy of the impact is used to disperse the fragments).



Using this energy density it is possible to estimate the mass of the target (Davis *et al.* 1989)

$$f_l = 0.5 \left( \frac{2SM}{\rho E} \right)^{1.24} \quad (3)$$

where  $S$ ,  $M$  and  $\rho$  is the impact strength, mass and density of the target respectively,  $E = (1/2)mv^2$  is the kinetic energy of the impactor and  $f_l$  is the mass ratio of the largest remaining fragment to the target. Using U XVII Sycorax as the largest remaining fragment and the energy needed to disperse U XVI Caliban to its present position we get a progenitor with a diameter of  $\sim 395\text{km}$ , assuming the progenitor was an icy body with impact strength  $S/\rho \sim 30\text{J/kg}$ . The mass ratio of U XVII Sycorax to the progenitor is  $f_l \sim 0.16$ .

This implies that the Uranian irregular satellites could be the remains a fractured natural satellite or a large captured Centaur/Trans-Neptunian Object. However, assuming a size distribution given by power-law (Greenberg *et al.* 1978)

$$N(> m) = Cm^{-b} \quad (4)$$

where  $N$  is the number of fragments with mass larger than  $m$ , and  $C$  and  $b$  are constants that can be determined through the total mass of the target  $M$  and the size of the largest fragment. Applying this to the Uranian system yields a distribution with 5-6 fragments with mass equal to or larger than U XVI Caliban. The stable region around Uranus has been searched to a  $\sim 90\%$  efficiency to a  $50\%$  “completeness magnitude” of  $m_R \sim 24.3 - 25.1$  (Gladman *et al.* 1998, 2000). Given U XVI Calibans magnitude,  $m_R = 21.9 \pm 0.1$  (Gladman *et al.* 1998), it is hard to imagine that the “missing” three or four fragments would have been missed in these searches. The one dynamical cluster hypothesis therefore looks unlikely.

## 6. Conclusion

The observations presented in this paper provide a survey of BVRI magnitudes and colors for 13 Jovian and 8 Saturnian irregular satellites. The results show that the irregular satellites seem to be divided into two classes based on colors. To avoid adding confusion with other terminology used in the field, the names of these two classes of have been chosen as **grey** and **light red**. Observations of additional objects are needed to confirm this division.

The colors of the irregular satellites found in this survey confirm that both C- and P/D-type asteroids are the most likely captured parent bodies, although at least one (J XXIII Kalyke) has colors too red for it to be a P/D-type asteroid. This indicates that it is possible that one or more Centaur/TNO have also been involved in the capture and fragmentation process, or some of the irregular satellites have experienced significant surface evolution.

The data also show a correlation between physical and dynamical properties in most of the clusters. This suggest that most clusters are the products of cratering or catastrophic fragmentation events. We also found that two of the dynamical clusters (the Jovian  $145^\circ$  and the Saturnian Phoebe cluster) have heterogeneous colors. The diverse and highly populated Jovian  $145^\circ$  cluster seems to most likely be the result of two (or maybe even three) cratering/fragmentation events. The existence of secular resonances in the region (Saha and Tremaine 1993; Carruba *et al.* 2002; Cúk *et al.* 2002) is good evidence that significant orbital evolution has occurred after the cratering/fragmentation events.

The S IX Phoebe cluster was also found to be heterogeneous and we show through a simplified analysis of possible cratering/fragmentation scenarios and subsequent dispersion velocities that these fragments are most likely two rather than one dynamical cluster, one centered on S IX Phoebe and another centered on S/2000 S 1. It is from this analysis not

possible to determine which of these two clusters the other Saturnian irregular satellites in the area (S/2000 S 7, S/2000 S 9 and S/2000 S 12) originated from. Study of the physical properties of these three satellites should help determine if they are part of the **light red** colored S/2000 S 1 cluster or the **neutral** colored S IX Phoebe cluster. It should also be noted that Buratti *et al.* (2002) suggest that the dark leading side of Iapetus and the surface of Hyperion are being coated by particles from retrograde satellites exterior to Iapetus' orbit. They determined that the visual spectra taken of the two surfaces can be explained as a linear admixture of two components: an icy satellite in the Saturnian system and a D-type asteroid. S IX Phoebe's visual spectral properties are unlike those of either Iapetus or Hyperion, so S IX Phoebe does not apparently contribute to the darkening of Iapetus's leading side. However, the colors determined for S/2000 S 1 show that it is consistent with a D-type asteroid and could therefore play a role in the darkening of Iapetus.

We also used the simple cratering/fragmentation analysis and showed that the six known Uranian irregular satellites can be divided into two dynamical cluster, one centered on U XVI Caliban and another on U XVII Sycorax, although there is an unlikely possibility that all six are fragments of a catastrophic fragmentation of a large (diameter of  $\sim 430\text{km}$ ) natural moon or captured Centaur/TNO.

In future studies we will determine BVRI colors of the irregular satellites not observed in this paper in order to help distinguish between the different dynamical clusters. Determining the colors of the remaining known Saturnian irregulars with inclinations around  $174^\circ$  is especially important. We will also investigate the near-IR JHK-bands to extend the spectral baseline, which will help in distinguishing the surface properties between objects with similar BVRI colors. This will help to classify the large and confusing set of Jovian irregulars in the  $140^\circ - 160^\circ$  inclination area.

## 7. Acknowledgments

This work has been supported by a Smithsonian Astrophysical Observatory Pre-doctoral Fellowship at the Harvard-Smithsonian Center for Astrophysics, Cambridge, USA.

We thank Brian Marsden and Gareth Williams of the Minor Planet Center for providing ephemerides, and Kris Stanek for his willingness to answer questions about photometry.

T. Grav was a visiting astronomer at the Nordic Optical Telescope. The Nordic Optical Telescope is operated on the island of La Palma jointly by Denmark, Finland, Iceland, Norway and Sweden, in the Spanish Observatorio del Roque de los Muchachos of the Instituto de Astrofísica de Canarias. Part of the data presented here have been taken using ALFOSC, which is owned by the Instituto de Astrofísica de Andalucía (IAA) and operated at the Nordic Optical Telescope under agreement between IAA and the NBIfAFG of the Astronomical Observatory of Copenhagen.

T. Grav and M.Holman were visiting astronomers at the MMT. The MMT is a joint facility owned by the Smithsonian Institution and the University of Arizona, and is located on Mt. Hopkins, Arizona.

T. Grav and M.Holman were visiting astronomers at the Magellan Baade Telescope. The Magellan Observatory is a collaboration between the Carnegie Observatories, the University of Arizona, Harvard University, University of Michigan, and MIT. The Magellan Observatory are located at Las Campanas Observatory, Chile, and operated by OCIW.

---

## REFERENCES

- Bowell, E., B. Hapke, D. Domingue, K. Lumme, J. Peltoniemi, and A. W. Harris 1989. Application of photometric models to asteroids. In *Asteroids II*, pp. 524–556.
- Buratti, B. J., M. D. Hicks, K. A. Tryka, M. S. Sittig, and R. L. Newburn 2002. High-Resolution 0.33-0.92  $\mu\text{m}$  Spectra of Iapetus, Hyperion, Phoebe, Rhea, Dione, and D-Type Asteroids: How Are They Related? *Icarus* **155**, 375–381.
- Byl, J., and M. W. Ovenden 1975. On the satellite capture problem. *MNRAS* **173**, 579–584.
- Carruba, V., J. A. Burns, P. D. Nicholson, M. Cuk, and R. A. Jacobson 2002. S2000S5 and S/2000S6: Saturnian moons trapped in the Kozai resonance. *AAS/Division for Planetary Sciences Meeting* **34**.
- Colombo, G., and F. A. Franklin 1971. On the formation of the outer satellite groups of Jupiter. *Icarus* **15**, 186–189.
- Cúk, M., and J. A. Burns 2001. Gas-Assisted Capture of the Irregular Satellites of Jupiter. *AAS/Division for Planetary Sciences Meeting* **33**.
- Cúk, M., J. A. Burns, V. Carruba, P. D. Nicholson, and R. A. Jacobson 2002. New Secular Resonances Involving the Irregular Satellites of Saturn. *AAS/Division of Dynamical Astronomy Meeting* **33**.
- Dacosta, G. S. 1992. Basic Photometry Techniques. In *ASP Conf. Ser. 23: Astronomical CCD Observing and Reduction Techniques*, pp. 90–104.
- Dahlgren, M., C.-I. Lagerkvist, A. Fitzsimmons, I. P. Williams, and M. Gordon 1997. A study of Hilda asteroids. II. Compositional implications from optical spectroscopy. *A&A* **323**, 606–619.

- Davis, D. R., S. J. Weidenschilling, P. Farinella, P. Paolicchi, and R. P. Binzel 1989. Asteroid collisional history - Effects on sizes and spins. In *Asteroids II*, pp. 805–826.
- Degewij, J. 1980. Spectroscopy of faint asteroids, satellites, and comets. *AJ* **85**, 1403–1412.
- Degewij, J., D. P. Cruikshank, and W. K. Hartmann 1980. Near-infrared colorimetry of J6 Himalia and S9 Phoebe - A summary of 0.3- to 2.2-micron reflectances. *Icarus* **44**, 541–547.
- Degewij, J., B. Zellner, and L. E. Andersson 1980. Photometric properties of outer planetary satellites. *Icarus* **44**, 520–540.
- Fujiwara, A., P. Cerroni, D. Davis, E. Ryan, and M. di Martino 1989. Experiments and scaling laws for catastrophic collisions. In *Asteroids II*, pp. 240–265.
- Gladman, B., and H. Boehnhardt 2000. S/1999 J 1. *IAU Circ.* **7472**, 2.
- Gladman, B., J. Kavelaars, M. Holman, J.-M. Petit, H. Scholl, P. Nicholson, and J. A. Burns 2000. NOTE: The Discovery of Uranus XIX, XX, and XXI. *Icarus* **147**, 320–324.
- Gladman, B., J. J. Kavelaars, M. Holman, P. D. Nicholson, J. A. Burns, C. W. Hergenrother, J. Petit, B. G. Marsden, R. Jacobson, W. Gray, and T. Grav 2001. Discovery of 12 satellites of Saturn exhibiting orbital clustering. *Nature* **412**, 163–166.
- Gladman, B. J., P. D. Nicholson, J. A. Burns, J. J. Kavelaars, B. G. Marsden, G. V. Williams, and W. B. Offutt 1998. Discovery of two distant irregular moons of Uranus. *Nature* **392**, 897–899.
- Green, D. W. E. 2002. Satellites of Jupiter. *IAU Circ.* **7998**, 2.
- Greenberg, R., W. K. Hartmann, C. R. Chapman, and J. F. Wacker 1978. Planetesimals to planets - Numerical simulation of collisional evolution. *Icarus* **35**, 1–26.

- Hartmann, W. K., D. P. Cruikshank, and J. Degewij 1982. Remote comets and related bodies - VJHK colorimetry and surface materials. *Icarus* **52**, 377–408.
- Heppenheimer, T. A. 1975. On the presumed capture origin of Jupiter’s outer satellites. *Icarus* **24**, 172–180.
- Heppenheimer, T. A., and C. Porco 1977. New contributions to the problem of capture. *Icarus* **30**, 385–401.
- Holman, M., J. Kavelaars, D. Milisavljevic, B. Gladman, P. Nicholson, C. Dumas, J.-M. Petit, B. G. Marsden, P. Rousselot, O. Mousis, and T. Grav 2002. S/2001 U 1. *IAU Circ.* **7980**, 1.
- Howell, S. B. 1989. Two-dimensional aperture photometry - Signal-to-noise ratio of point-source observations and optimal data-extraction techniques. *PASP* **101**, 616–622.
- Jarvis, K. S., F. Vilas, S. M. Larson, and M. J. Gaffey 2000. JVI Himalia: New compositional evidence and interpretations for the origin of Jupiter’s small satellites. *Icarus* **145**, 445–453.
- Kuiper, G. P. 1956. On the origin of the satellites and the Trojans. *Vistas in Astronomy* **2**, 1631–1666.
- Landolt, A. U. 1992. Broadband UBVRI photometry of the Baldwin-Stone Southern Hemisphere spectrophotometric standards. *AJ* **104**, 372–376.
- Lassell, W. 1846. Discovery of supposed ring and satellite of Neptune . *MNRAS* **7**, 157.
- Luu, J. 1991. CCD photometry and spectroscopy of the outer Jovian satellites. *AJ* **102**, 1213–1225.

- Maris, M., G. Carraro, G. Cremonese, and M. Fulle 2001. Multicolor Photometry of the Uranus Irregular Satellites Sycorax and Caliban. *AJ* **121**, 2800–2803.
- McLeod, B. A., M. Conroy, T. M. Gauron, J. C. Geary, and M. P. Ordway 2000. Megacam: A Wide-field Imager for the MMT Observatory. In *Further Developments in Scientific Optical Imaging*, pp. 11.
- Pollack, J. B., J. A. Burns, and M. E. Tauber 1979. Gas drag in primordial circumplanetary envelopes - A mechanism for satellite capture. *Icarus* **37**, 587–611.
- Rettig, T. W., K. Walsh, and G. Consolmagno 2001. Implied Evolutionary Differences of the Jovian Irregular Satellites from a BVR Color Survey. *Icarus* **154**, 313–320.
- Romon, J., C. de Bergh, M. A. Barucci, A. Doressoundiram, J.-G. Cuby, A. Le Bras, S. Douté, and B. Schmitt 2001. Photometric and spectroscopic observations of Sycorax, satellite of Uranus. *A&A* **376**, 310–315.
- Roy, A. E. 1988. *Orbital motion*. Bristol, England ; Philadelphia : A. Hilger, 1988. 3rd ed.
- Saha, P., and S. Tremaine 1993. The orbits of the retrograde Jovian satellites. *Icarus* **106**, 549–562.
- Sawyer, S. R. 1991. *A High-Resolution CCD Spectroscopic Survey of Low-Albedo Main Belt Asteroids*. Ph. D. thesis.
- Schaefer, B. E., and M. W. Schaefer 2000. Nereid Has Complex Large-Amplitude Photometric Variability. *Icarus* **146**, 541–555.
- Scotti, J. V., T. B. Spahr, R. S. McMillan, J. A. Larsen, J. Montani, A. E. Gleason, T. Gehrels, B. G. Marsden, and G. V. Williams 2000. S/1999 J 1. *IAU Circ.* **7460**, 1.



- Sheppard, S. S., D. C. Jewitt, Y. Fernandez, G. Magnier, B. G. Marsden, M. Holman, C. T. Kowal, E. Roemer, and G. V. Williams 2000. S/1975 J 1 = S/2000 J 1. *IAU Circ.* **7525**, 1.
- Sheppard, S. S., D. C. Jewitt, Y. R. Fernandez, G. Magnier, B. G. Marsden, S. Dahm, and A. Evans 2001. Satellites of Jupiter. *IAU Circ.* **7555**, 1.
- Sheppard, S. S., D. C. Jewitt, J. Kleyna, B. G. Marsden, and R. Jacobson 2002. Satellites of Jupiter. *IAU Circ.* **7900**, 1.
- Simonelli, D. P., J. Kay, D. Adinolfi, J. Veverka, P. C. Thomas, and P. Helfenstein 1999. Phoebe: Albedo Map and Photometric Properties. *Icarus* **138**, 249–258.
- Sørensen, N. A., and P. Nørregaard 1996. The ALFOSC camera, properties of the W11-3 CCD. Technical report, Copenhagen University Observatory.
- Stetson, P. B., L. E. Davis, and D. R. Crabtree 1990. Future development of the DAOPHOT crowded-field photometry package. In *ASP Conf. Ser. 8: CCDs in astronomy*, pp. 289–304.
- Sykes, M. V., B. Nelson, R. M. Cutri, D. J. Kirkpatrick, R. Hurt, and M. F. Skrutskie 2000. Near-Infrared Observations of the Outer Jovian Satellites. *Icarus* **143**, 371–375.
- Tegler, S. C., and W. Romanishin 1998. Two distinct populations of Kuiper-belt objects. *Nature* **392**, 49.
- Tegler, S. C., and W. Romanishin 2000. Extremely red Kuiper-belt objects in near-circular orbits beyond 40 AU. *Nature* **407**, 979–981.
- Tholen, D. J., and B. Zellner 1983. Eight-color photometry of Hyperion, Iapetus, and Phoebe. *Icarus* **53**, 341–347.

Tholen, D. J., and B. Zellner 1984. Multicolor photometry of outer Jovian satellites.

*Icarus* **58**, 246–253.

Tody, D. 1986. The IRAF Data Reduction and Analysis System. In *Instrumentation in astronomy VI; Proceedings of the Meeting, Tucson, AZ, Mar. 4-8, 1986. Part 2 (A87-36376 15-35)*. Bellingham, WA, Society of Photo-Optical Instrumentation Engineers, 1986, p. 733., Volume 627, pp. 733.

Tody, D. 1993. IRAF in the Nineties. In *ASP Conf. Ser. 52: Astronomical Data Analysis Software and Systems II*, Volume 2, pp. 173.

### Table Caption

Table 1 Here are shown the observational circumstances for each object. OPT is the Observer-Primary-Target angle.

Table 2 Here are shown the photometric results of the observations. The  $m_v(1, 1, 0)$  gives the absolute magnitude normalized to unit heliocentric and geocentric distances, and zero phase angle.  $1\sigma$  errors are given.

### Figure Caption

Figure 1. The  $B - V$  vs.  $V - I$  plot of all available photometry of irregular satellites. Photometry of J VI Himalia, J VII Elara, J XIII Leda is from Rettig *et al.* (2001) and the two Uranian U XVI Caliban and U XVII Sycorax can be found in Maris *et al.* (2001); Romon *et al.* (2001). The color of N II Nereid can be found in Schaefer and Schaefer (2000). Note that J XX Taygete and S/2000 S 1 have identical  $B - V$  and  $V - I$  colors.

Figure 2. The same as Fig. 1, but showing the  $B - V$  vs.  $V - I$  colors.

Figure 3. The same as Fig. 1, but showing the  $V - R$  vs.  $V - I$  colors.

Figure 4. The same as Fig. 1 but also containing the known Centaurs and TNOs with photometry better than 0.05 magnitude. It is seen that the colors of the irregular satellites are similar to the *grey* class of the Centaurs and TNOs (Tegler and Romanishin 1998, 2000).

Figure 5. Here is shown the mean motion semimajor axis and inclination of the irregular satellites plotted in a polar plot normalized to the Hill-sphere radius of the satellite's parent planet. The irregular satellites for which colors have been determined is plotted in color depending on which color class we put it in, *blue* for **grey** and *red* for **light red**. The colored ellipses give the area of a-i phase space were each cluster could disperse to

given an catastrophic event which gives the fragments speeds of 135m/s for J VI Himalia, 30m/s for J XI Carme, 50m/s for the Saturnian 34° cluster, 350m/s for the Saturnian 45° cluster, 200m/s for the S IX Phoebe, 120m/s for the Saturnian 174° cluster, 75m/s and fragmentation at  $M = 180^\circ$  for U XVI Caliban, and 120m/s and fragmentation at  $M = 80^\circ$  for U XVII Sycorax. The region within which the the Kozai mechanism drives orbits to eccentricities high enough for the objects to penetrate into the regular satellites is indicated by the dashed lines for each planet (Gladman *et al.* 2001).

Object	Telescope	UT Date	R (AU)	$\Delta$ (AU)	$\alpha$ ( $^{\circ}$ )	OPT ( $^{\circ}$ )
Pasiphae	Magellan-6.5m	2002 Feb. 12.	5.10	4.37	8.01	47.5
Sinope	NOT-2.56m	2002 Jan. 14.	5.30	4.33	2.35	124.3
Lysithea	Magellan-6.5m	2002 Feb. 12.	5.18	4.46	8.14	89.3
Carme	NOT-2.56m	2002 Mar. 14.	5.18	4.86	10.75	73.0
Ananke	NOT-2.56m	2002 Mar. 14.	5.11	4.82	10.99	33.2
Callirrhoe	Magellan-6.5m	2002 Feb. 09.	5.34	4.58	7.23	153.9
Themisto	Magellan-6.5m	2002 Feb. 12.	5.16	4.44	8.10	64.6
Kalyke	NOT-2.56m	2002 Jan. 14.	5.04	4.09	3.16	41.8
	MMT-6m	2002 Mar. 13.	5.05	4.73	11.06	22.5
Iocaste	Magellan-6.5m	2002 Feb. 09.	5.06	4.31	7.89	35.0
Harpalyke	NOT-2.56m	2002 Jan. 14.	5.15	4.20	3.11	80.4
Praxidike	Magellan-6.5m	2002 Feb. 12.	5.06	4.33	8.11	30.1
Magaclite	NOT-2.56m	2002 Jan. 14.	5.17	4.21	2.27	85.2
Taygete	Magellan-6.5m	2002 Feb. 09.	5.02	4.27	7.94	21.4
Phoebe	NOT-2.56m	2001 Feb. 18.	9.08	9.13	6.21	76.4
S/2000 S1	Magellan-6.5m	2002 Feb. 09.	9.20	8.86	5.86	158.6
S/2000 S2	NOT-2.56m	2002 Jan. 13.	9.06	8.33	4.36	85.9
S/2000 S3	NOT-2.56m	2002 Jan. 13.	8.93	8.22	4.49	39.1
S/2000 S4	NOT-2.56m	2002 Jan. 14.	8.95	8.22	4.40	50.3
S/2000 S5	NOT-2.56m	2002 Mar. 14.	9.03	9.23	6.12	62.8
S/2000 S10	MMT-6m	2002 Mar. 13.	8.93	9.11	6.21	39.7
S/2000 S11	NOT-2.56m	2001 Feb. 18.	9.18	9.23	6.15	120.8
	NOT-2.56m	2002 Jan. 14.	9.04	8.31	4.39	66.0

Table 1: Grav et al., Photometric Survey of Irregular Satellites

Object	Inclination	$m_V$ (1,1,0)	V	B-V	V-R	V-I
Lysithea	28.3°	11.09 ± 0.02	18.48 ± 0.02	0.72 ± 0.02	0.36 ± 0.02	0.74 ± 0.02
Themisto	43.1°	12.94 ± 0.01	20.31 ± 0.01	0.83 ± 0.02	0.46 ± 0.01	0.94 ± 0.02
Callirrhoe	147.1°	13.92 ± 0.02	21.39 ± 0.02	0.72 ± 0.03	0.50 ± 0.02	1.02 ± 0.02
Harpalyke	148.7°	16.03 ± 0.12	23.02 ± 0.12		0.43 ± 0.17	0.62 ± 0.22
Praxidike	148.7°	15.24 ± 0.03	22.51 ± 0.03	0.77 ± 0.06	0.34 ± 0.03	0.74 ± 0.04
Ananke	148.9°	11.87 ± 0.03	19.51 ± 0.03	0.90 ± 0.06	0.38 ± 0.04	0.86 ± 0.04
Iocaste	149.7°	15.27 ± 0.03	22.52 ± 0.03	0.63 ± 0.06	0.36 ± 0.04	0.62 ± 0.05
Pasiphae	151.4°	9.92 ± 0.01	17.22 ± 0.01	0.74 ± 0.01	0.38 ± 0.01	0.74 ± 0.01
Magaelite	152.7°	15.12 ± 0.05	22.07 ± 0.05	0.94 ± 0.09	0.41 ± 0.07	1.05 ± 0.07
Sinope	158.1°	11.56 ± 0.02	18.63 ± 0.02	0.84 ± 0.03	0.46 ± 0.03	0.93 ± 0.04
Carme	164.9°	10.91 ± 0.02	18.59 ± 0.02	0.76 ± 0.02	0.47 ± 0.02	0.97 ± 0.02
Kalyke	165.2°	15.42 ± 0.07	22.31 ± 0.07		0.72 ± 0.09	0.96 ± 0.16
		15.28 ± 0.04	22.86 ± 0.04	0.94 ± 0.08	0.70 ± 0.05	0.88 ± 0.06
Taygete	165.2°	15.63 ± 0.04	22.85 ± 0.04	0.56 ± 0.08	0.52 ± 0.04	0.96 ± 0.05
S/2000 S4	33.5°	12.56 ± 0.06	22.28 ± 0.06	0.77 ± 0.12	0.57 ± 0.09	0.88 ± 0.11
S/2000 S11	34.0°	10.88 ± 0.03	21.00 ± 0.03	0.89 ± 0.07	0.50 ± 0.05	0.91 ± 0.05
		11.20 ± 0.03	20.97 ± 0.03	0.98 ± 0.07	0.47 ± 0.04	0.92 ± 0.04
S/2000 S10	34.5°	13.90 ± 0.06	23.90 ± 0.05	0.83 ± 0.09	0.49 ± 0.06	0.61 ± 0.12
S/2000 S2	45.1°	11.83 ± 0.03	21.61 ± 0.03	0.77 ± 0.06	0.48 ± 0.05	0.94 ± 0.04
S/2000 S3	45.6°	10.69 ± 0.02	20.38 ± 0.02	0.80 ± 0.04	0.52 ± 0.03	0.96 ± 0.04
S/2000 S5	46.2°	12.65 ± 0.12	22.73 ± 0.12	0.87 ± 0.22	0.66 ± 0.15	0.97 ± 0.17
S/2000 S1	173.1°	12.39 ± 0.03	22.41 ± 0.03	0.56 ± 0.05	0.52 ± 0.04	0.96 ± 0.05
Phoebe	174.8°	6.63 ± 0.01	16.71 ± 0.01	0.63 ± 0.01	0.35 ± 0.01	0.64 ± 0.01

Table 2: Grav et al., Photometric Survey of Irregular Satellites

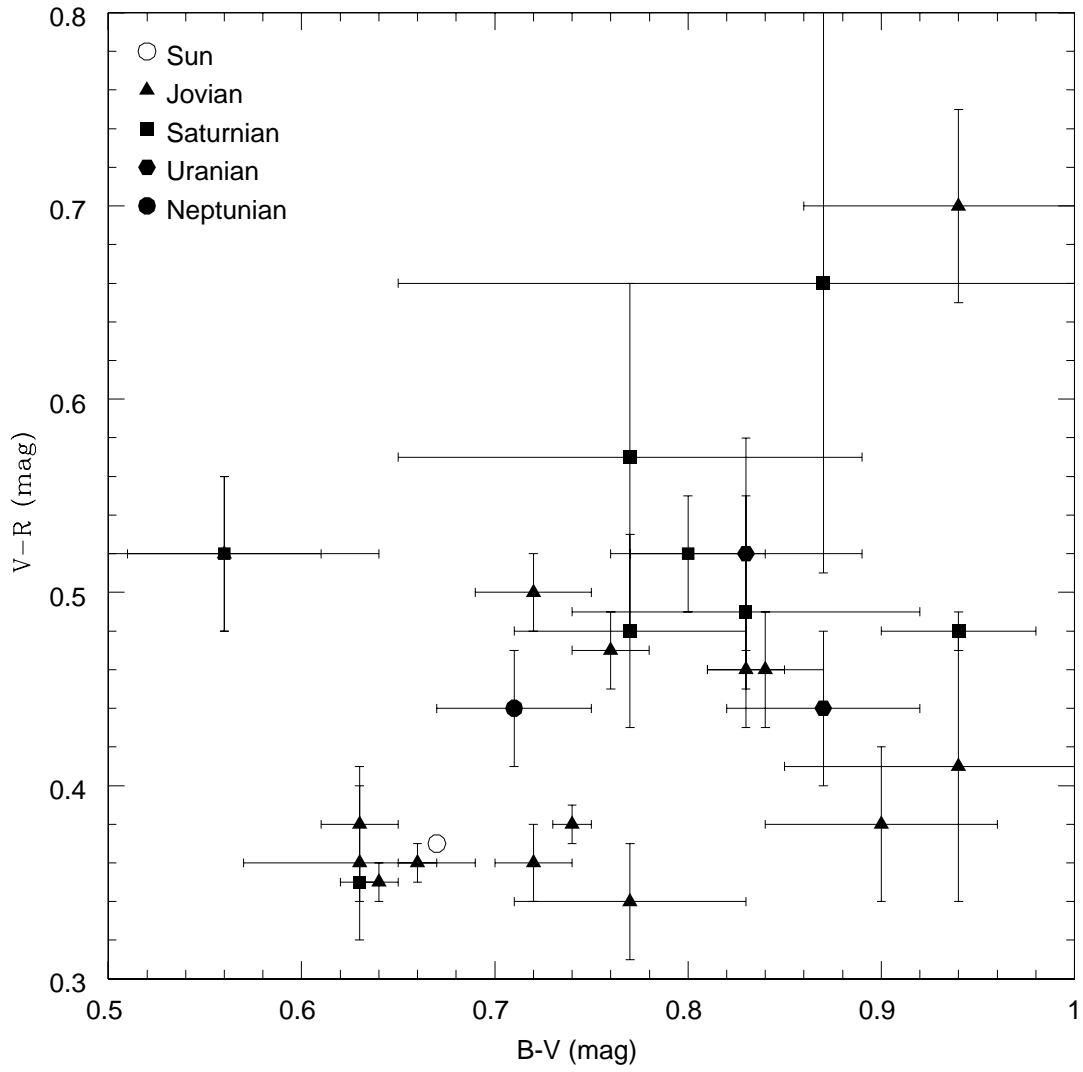


Fig. 1.— Grav et al., Photometric Survey of Irregular Satellites

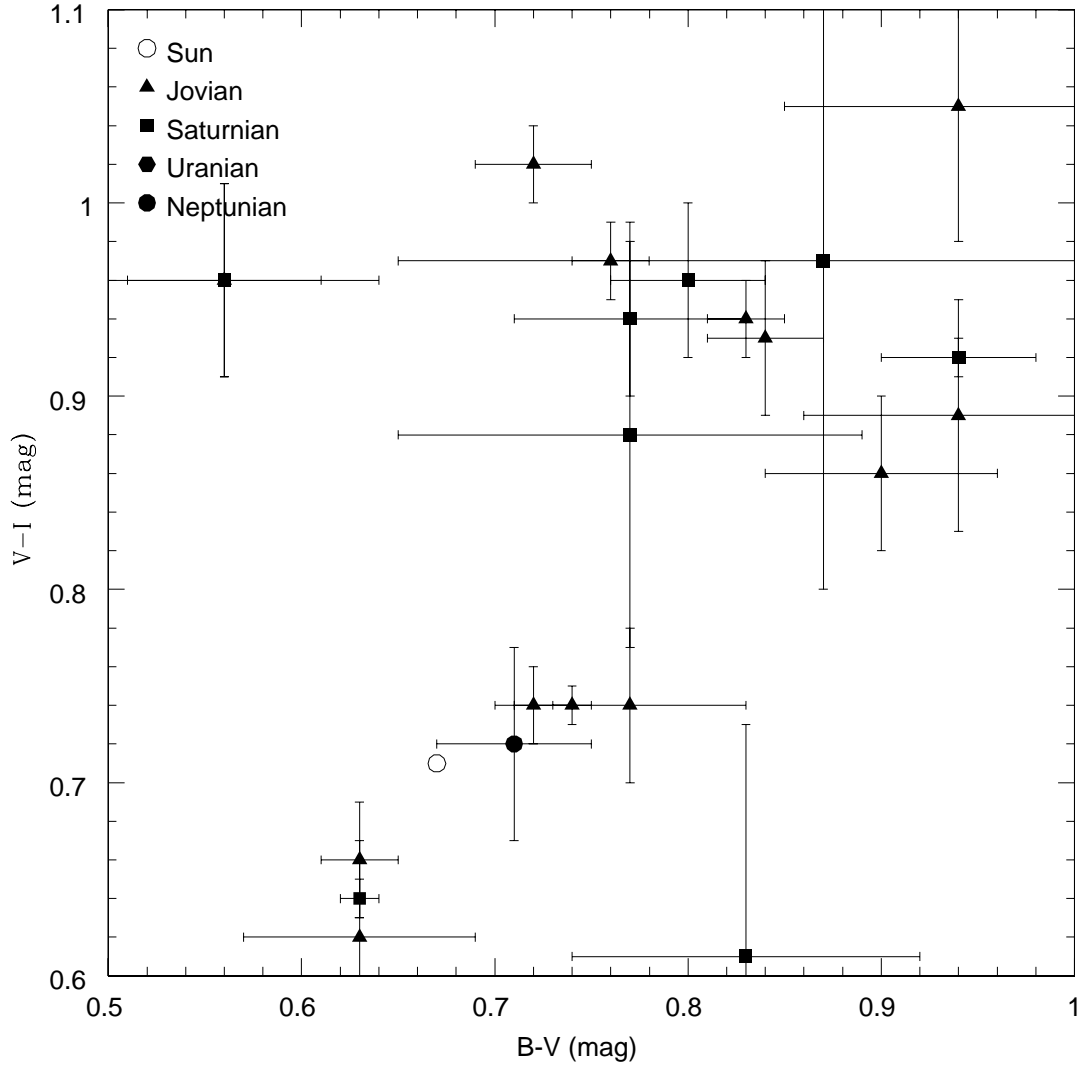


Fig. 2.— Grav et al., Photometric Survey of Irregular Satellites



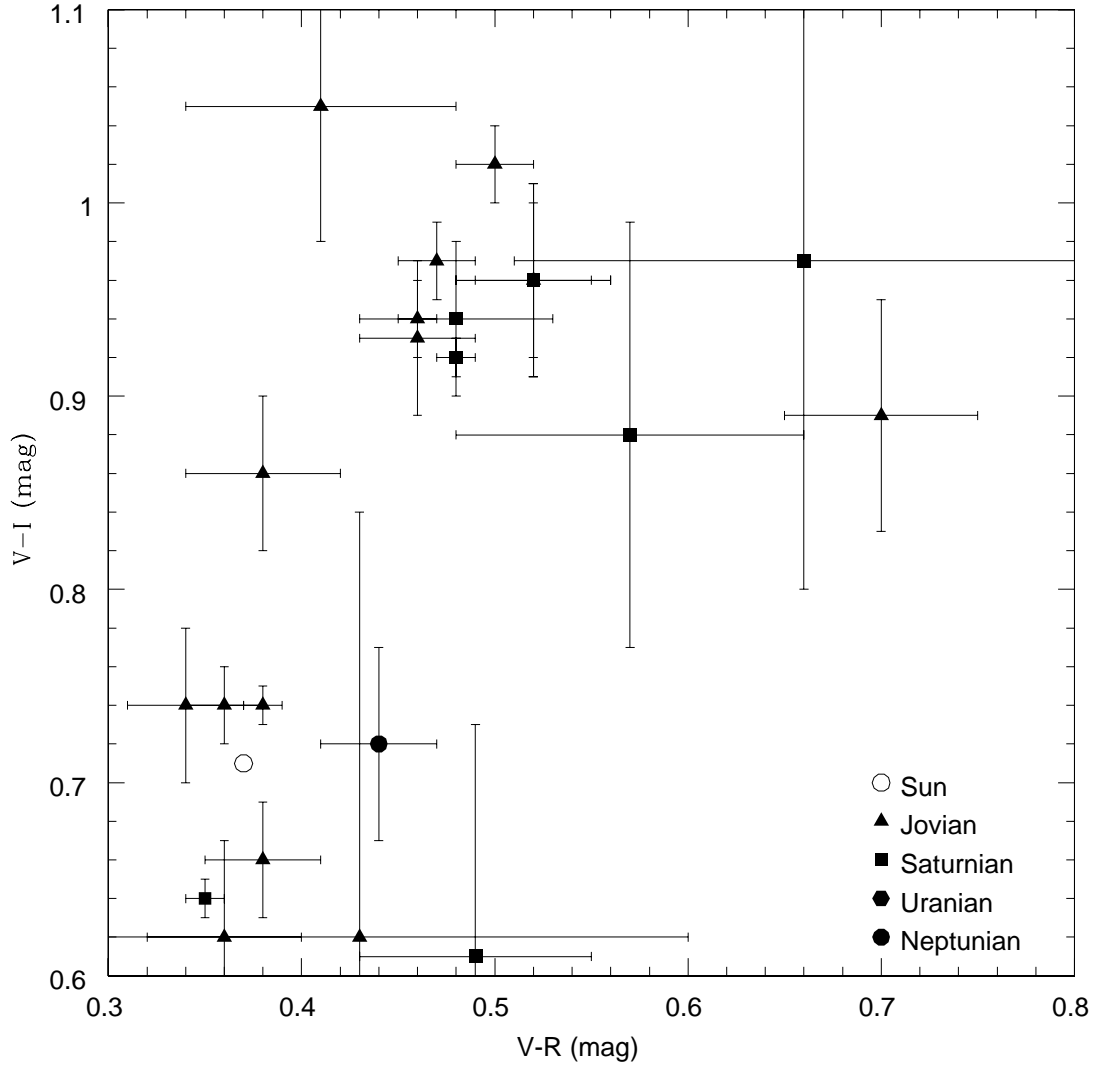


Fig. 3.— Grav et al., Photometric Survey of Irregular Satellites

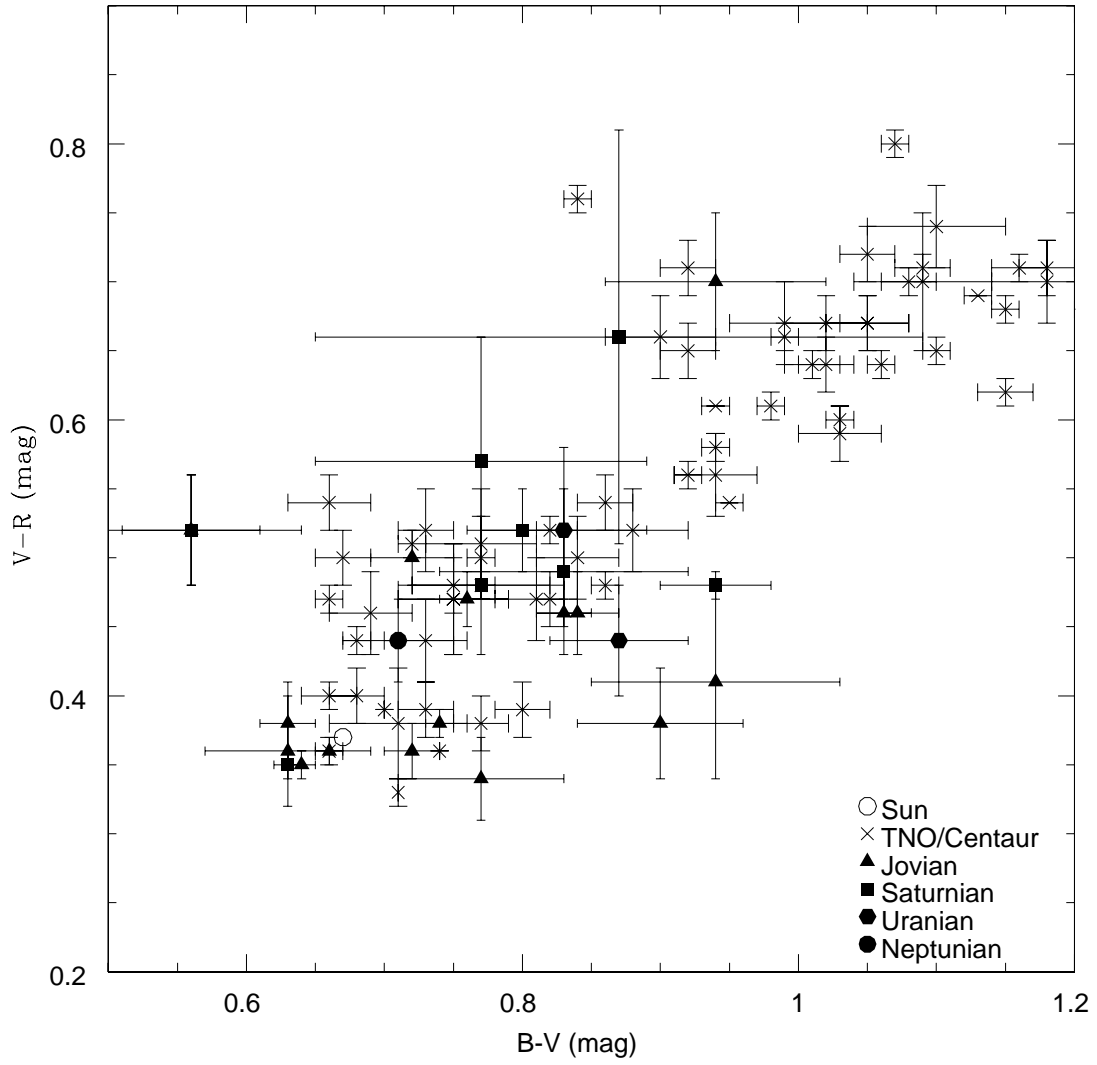


Fig. 4.— Grav et al., Photometric Survey of Irregular Satellites

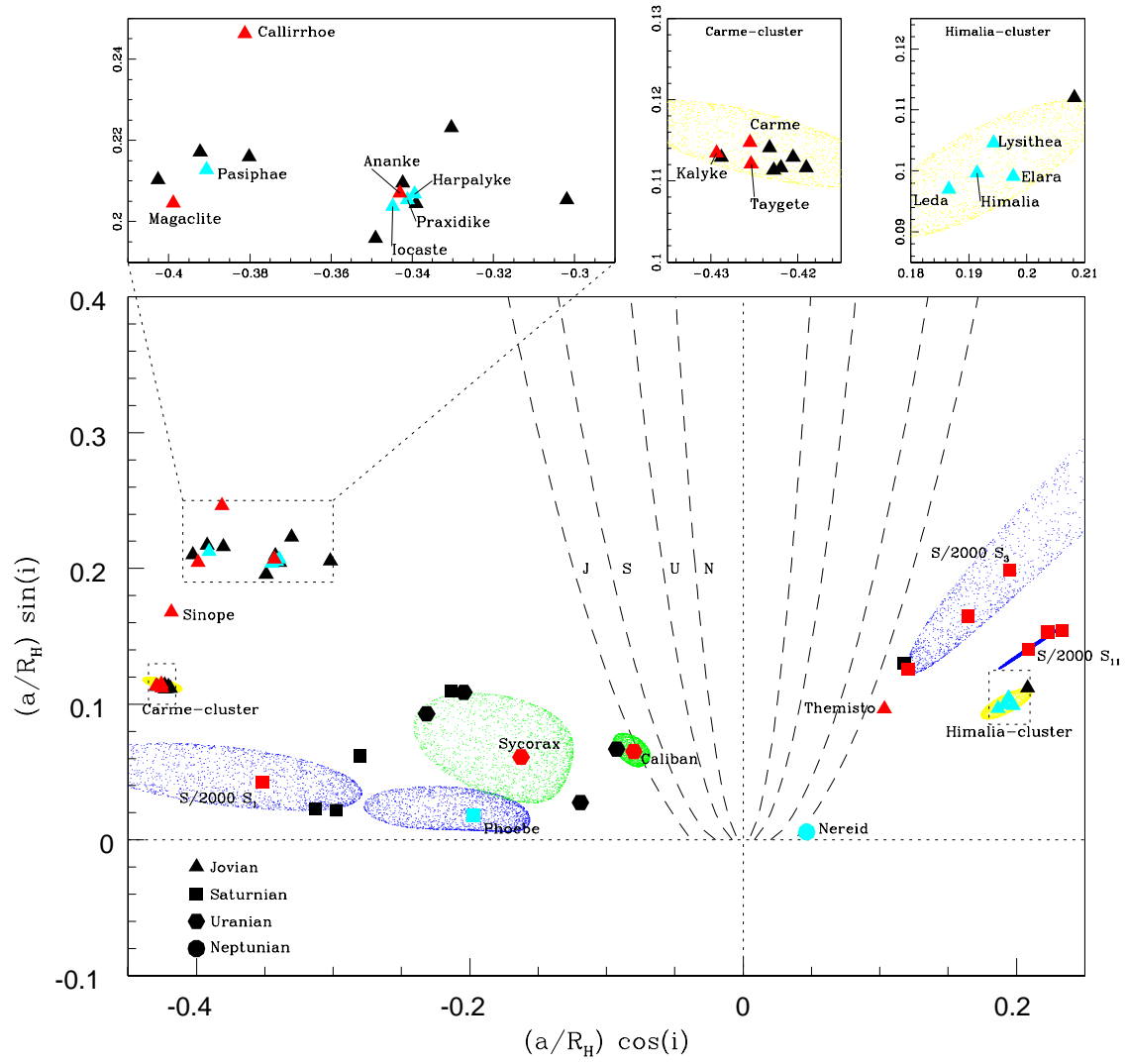


Fig. 5.— Grav et al., Photometric Survey of Irregular Satellites